

## Crystal chemical investigations of epidote group minerals from two Bulgarian localities: Effects of Mn content and Mn/Fe ratio on the structural peculiarities

Vladislav Kostov-Kytin<sup>1</sup>, Rositsa Nikolova<sup>1</sup>, Sylvina Georgieva<sup>2</sup>,  
Ivayla Sopotenska<sup>3</sup>, Milen Kadiyski<sup>3</sup>, Rossitsa Vassileva<sup>2</sup>

<sup>1</sup> Institute of Mineralogy and Crystallography, Bulgarian Academy of Sciences, Acad. G. Bonchev Str., Bl. 107, 1113 Sofia, Bulgaria; e-mails: vkytin@abv.bg; rosica.pn@clmc.bas.bg

<sup>2</sup> Geological Institute, Bulgarian Academy of Sciences, Acad. G. Bonchev Str., Bl. 24, 1113 Sofia, Bulgaria; e-mails: rosivas@geology.bas.bg; sylvina@geology.bas.bg

<sup>3</sup> Aurubis Bulgaria AD, Research and Development, Industrial Zone Pirdop, Bulgaria; e-mail: m.kadiyski@aurubis.com

(Received: 27 August 2023; accepted in revised form: 10 October 2023)

**Abstract.** The current study presents results of crystal chemical studies of epidote samples from two Central Rhodope localities. Based on the obtained crystal chemical information, the nomenclature of the investigated species has been justified within the IMA-recommended nomenclature of epidote-group minerals. A comparative study has also been accomplished, including data from the present study as well as literature data from selected epidotes possessing similar crystal structural peculiarities. Certain trends have been derived from the transition metal(s) type and content(s) in the most distorted of the three six-coordinated sites (designated as M3) on selected geometrical and crystallographic parameters. The impact of Mn content and Mn/Fe ratio on the structural peculiarities and coloration of the specimens containing this element are discussed in terms of manifestation of the Jahn-Teller effect on the herein-considered epidote phases.

Kostov-Kytin, V., Nikolova, R., Georgieva, S., Sopotenska, I., Kadiyski, M., Vassileva, R. 2023. Crystal chemical investigations of epidote group minerals from two Bulgarian localities: Effects of Mn content and Mn/Fe ratio on the structural peculiarities. *Geologica Balcanica* 52 (3), 95–109.

**Keywords:** Mn-containing epidotes, single-crystal X-ray diffraction, Central Rhodopes, Bulgaria.

### INTRODUCTION

The crystal structure of epidote was initially determined by Ito (1950) and later confirmed by Belov and Rumanova (1953) and Ito *et al.* (1954) by X-ray analyses. Single-crystal studies of monoclinic epidote varieties carried out in the following years have provided sufficient information about the compositional complexity and certain specific features

of the overall structural arrangement of these common rock-forming minerals. Epidotes are currently considered as a group of minerals described with the generic formula  $A_2M_3[T_2O_7][TO_4](O,F)(OH,O)$  by Armbruster *et al.* (2006). These authors described the monoclinic crystal structure as “composed of  $T_2O_7$  (usually  $Si_2O_7$ ) and  $TO_4$  (usually  $SiO_4$ ) units linked to two kinds of chains (parallel to the b-axis) built by edge-sharing octahedra. One chain consists

of M2 octahedra while the other chain is formed by M1 octahedra with M3 octahedra attached on alternate sides along its length... M2 has a strong preference for Al whereas the occupancy of M1 and M3 depends on competing ions. Usually an OH group is bonded to the M2 cation. The overall structural arrangement gives rise to two types of cavities, a smaller one named A1... and a larger one named A2... The resulting connectivity (topology) is consistent with space group  $P2_1/m$ " (see Fig. 1). Referring to earlier crystal-structural studies, Armbuster *et al.* (2006) made the following important clarifications: (i) monoclinic members of the epidote group have three distinct octahedral

sites (M1, M2, M3), each contributing with the same multiplicity to the formula; (ii) if all of these sites are found to be dominantly occupied by Al, such compound should be defined as clinozoisite; (iii) if by chance ferric iron did not order onto the largest and most distorted octahedral site M3, but were randomly distributed over the three available sites, the compound would have to be called *ferrian clinozoisite*, since Al would be dominant at all three octahedral sites (M1, M2, M3), even where its composition suggests that the total Fe content is equal or exceeds 1 apfu, *e.g.*,  $\text{Ca}_2\text{Al}_2\text{Fe}^{3+}[\text{Si}_2\text{O}_7][\text{SiO}_4]\text{O}(\text{OH})$ ; (iv) if Fe is the dominant cation in any of the octahedral sites (preferentially M3), then this is epidote.

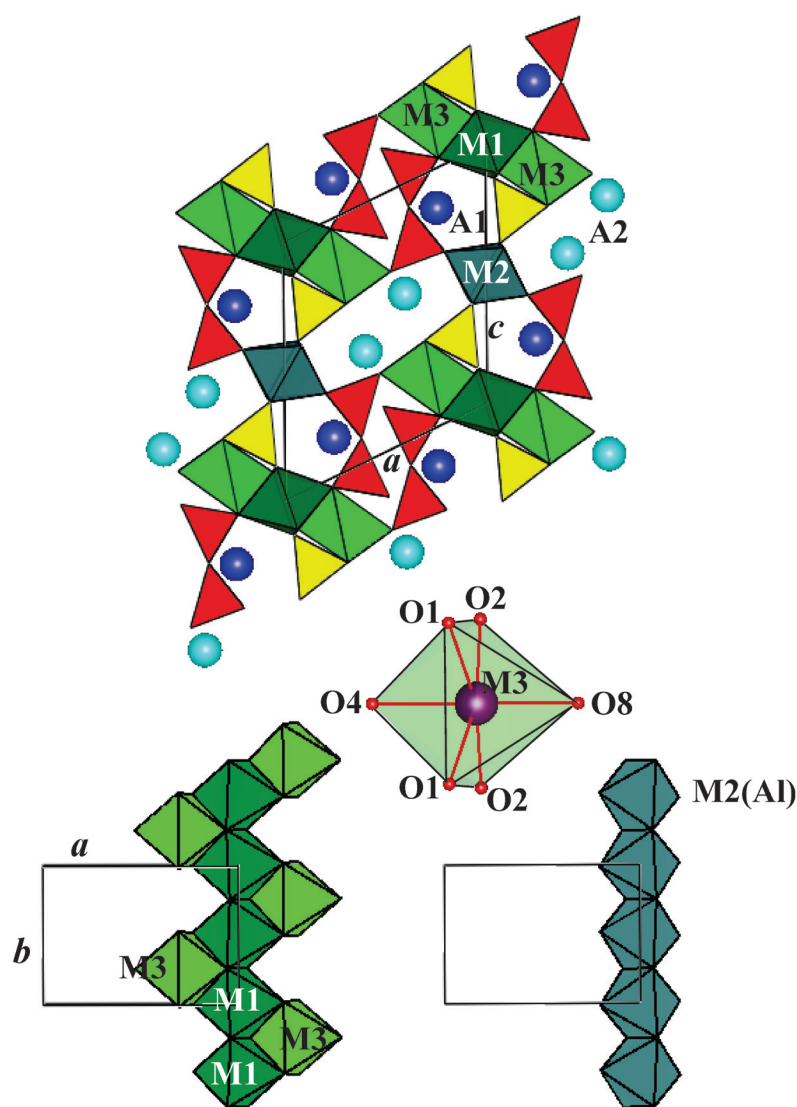


**Fig. 1.** Top: polyhedral model of the epidote structure (space group  $P2_1/m$ ) projected along the  $b$ -axis.  $\text{SiO}_4$  tetrahedra are presented in yellow;  $\text{Si}_2\text{O}_7$  groups in red, octahedra in green, A sites are shown as blue spheres (A1 dark blue, A2 light blue). Bottom: linkage of octahedral sites forming chains parallel to the  $b$ -axis. Middle: the M3 distorted octahedron coordination environment. The designations used follow those of Armbuster *et al.* (2006) and Dollase (1968).

Although not explicitly stated in this work, similar reasoning can be applied to the composition of manganese in these compounds as well as to the definition for piemontite. Again referring to previous researchers, Armbruster *et al.* (2006) noted that “there seems to be a general problem with the assignment of the name piemontite” and that “the compositions of most samples fall in the vicinity of Al:Mn = 2:1 with a general trend of some excess Mn extending to Al:Mn = 1.3:1.”

The website of the Hudson Institute of Mineralogy (mindat.org), respecting the notations of Armbruster *et al.* (2006), presents the following general formula of the epidote group sorosilicates, providing also brief characteristics of the cation sites in it:  $(A1^{2+}A2^{2+})(M1^{3+}M2^{3+}M3^{3+})O[Si_2O_7][SiO_4](OH)$ , where:

- A1 = large (variably VIII,IX,X)-coordinated site, usually occupied by Ca, less commonly  $Mn^{2+}$ ; limited vacancies have been reported;
- A2 = large (variably IX,X)-coordinated site (larger than A1), usually Ca, but also Y, REE, Sr, Pb; Th (especially) and U may be present; limited vacancies have been reported;
- M1 = VI-coordinated site, usually occupied by Al, but also sometimes  $Fe^{3+}$  and  $Mn^{3+}$ ; Cr is reportedly strongly partitioned into M1.
- M2 = VI-coordinated site, almost exclusively Al.
- M3 = most distorted of the three VI-coordinated sites, most commonly Al,  $Fe^{3+}$  and  $Mn^{3+}$ , but also V,  $Fe^{2+}$ ,  $Mn^{2+}$ , Mg, Cr (<https://www.mindat.org/min-46234.html>, <https://www.mindat.org/min-6662.html>; see Fig. 1).

Mindat.org distinguishes two series within the epidote group: clinozoisite-epidote series with ideal formula varying between its end-members from  $(CaCa)(AlAlAl)O[Si_2O_7][SiO_4](OH)$  to  $(CaCa)(AlAlFe^{3+})O[Si_2O_7][SiO_4](OH)$  (<https://www.mindat.org/min-8971.html>), and piemontite-epidote series with formulas from  $(CaCa)(AlAlFe^{3+})O[Si_2O_7][SiO_4](OH)$  to  $(CaCa)(AlAlMn^{3+})O[Si_2O_7][SiO_4](OH)$  (<https://www.mindat.org/min-470375.html>). Mindat.org also notes that piemontite (*sensu stricto*) is a mineral species with the formula  $(CaCa)(AlAlMn^{3+})O[Si_2O_7][SiO_4](OH)$ , “but more commonly ‘piemontite’ refers incorrectly to deep red colored,  $Mn^{3+}$ -bearing epidotes that are really varieties of the species epidote, and not strictly speaking piemontite. ‘Piemontites’ rarely contain more than 40% of the piemontite molecule, so many ‘piemontites’ in collections are really Mn-rich red varieties of epidote” (<https://www.mindat.org/min-3208.html>).

Regardless of the ambiguities in some mineral definitions, the crystal chemical studies so far

have proven indisputably that, in the epidote crystal structures, the largest and most distorted octahedral site M3 is a preferential location for cations with larger ionic radius than aluminum ( $R^{VI}Al^{3+} = 0.535 \text{ \AA}$ ; Shannon, 1976), *e.g.*, Fe and Mn. The M2 site is occupied exclusively by Al, whereas the M1 VI-coordinated site is sometimes reported to contain  $Fe^{3+}$  and  $Mn^{3+}$ . The ability of M1 to expand and consequently to accommodate significant quantities of  $Fe^{3+}$  is roughly related to the volume of the M3 polyhedron (Bonazzi and Menchetti, 1995). The latter authors reported that the amount of iron in M1 becomes significant only when the polyhedral volume of M3 (M3 PV) reaches about  $11 \text{ \AA}^3$ , *i.e.*, in epidotes when  $Fe^{3+}(M3) > 0.80 \text{ apfu}$ .

In most of the previous studies,  $Fe^{3+}$  and  $Mn^{3+}$  have been assumed to show the same behavior, because the ionic radii of  $Fe^{3+}$  and  $Mn^{3+}$  ( $R^{VI}Fe^{3+} = 0.645 \text{ \AA}$  and  $R^{VI}Mn^{3+} = 0.645 \text{ \AA}$  – Shannon, 1976; high spin configurations) are the same and Fe cannot be distinguished from Mn in X-ray structural analyses. However, Nagashima and Akasaka (2010) reported that “it is a challenge to investigate the specific influence of unique  $Fe^{3+}$  and  $Mn^{3+}$  substitution for Al on structural changes because natural epidote-group minerals commonly contain not only  $Fe^{3+}$  but also  $Mn^{3+}$ . Although  $Fe^{3+}$  and  $Mn^{3+}$  have similar ionic radii, their electronic configurations and induced distortions are different.” Summarizing results from previous investigations on the distribution of  $Fe^{3+}$  and  $Mn^{3+}$  among octahedral sites and the variations of structural changes caused by  $Fe^{3+}$  and  $Mn^{3+}$  substitution for Al, the latter authors stated that the variation of the unit-cell parameters with  $M^{3+}$  ( $M = Fe^{3+} + Mn^{3+}$ ) is not simple. They concluded that “It shows the combined result of linear variation due to  $Al \leftrightarrow Fe^{3+}$  substitution (Giuli *et al.* 1999) and nonlinear variation due to  $Al \leftrightarrow Mn^{3+}$  substitution (Nagashima and Akasaka 2004)”, the latter one being due to the Jahn-Teller effect.

The crystal chemistry and physics of trivalent manganese in minerals and other crystalline materials is greatly influenced by the Jahn-Teller effect (Jahn and Teller, 1937). The Jahn-Teller effect of the  $3d^4$ -configured  $Mn^{3+}$  in the M3 VI-coordinated site in the epidote group members that contain this element is manifested in the axial compression of its octahedral environment along the “octahedral apices” (ap), *i.e.*, O8-M3-O4 (Fig. 1). The symmetrically equivalent O1 and O2 atoms depicted in the same part of the figure form an “octahedral plane” designated hereinafter as equatorial (eq). This compression is more pronounced with the increase in  $Mn^{3+}$  content in this position and is absent in those

cases where only the spherically symmetrical  $3d^5$ -configured  $Fe^{3+}$  occupies it. More details on the Jahn-Teller effect of manganese in epidotes and other minerals can be found in Langer *et al.* (2002).

Thus, the M3 VI-coordinated site in the epidote structure is a preferred position for competing ions of various characteristics. Most commonly,  $Al^{3+}$ ,  $Fe^{3+}$  and  $Mn^{3+}$  populate it. Because of the difference in ionic radii and manifestation of the Jahn-Teller effect in manganese, the contents and ratios of these elements in M3 inevitably affect the geometry of the adjacent octahedral environment of this site and, consequently, other crystallographic and geometric parameters of the structure as a whole. This also concerns some physical properties, such as the color of the samples, for example. It is a well-known fact that  $Mn^{3+}$  is a strong chromophore contributing to the saturated pink, red, and red-violet coloration of epidote representatives, even when manganese content is very low. Such are some natural and synthetic orthozoisite-type “thulites” and clinozoisite-type piemontites (Langer *et al.*, 2002).

The present work consists of two parts. The first one presents new crystal chemical data on Mn-bearing varieties of the epidote group of minerals from two Bulgarian localities in the Central Rhodopes (diopside-scapolite marbles from Samurski Dol, Arda Unit, and altered pegmatite in the area of the Pechinsko Pass, near the Strashimir Pb-Zn vein deposit, Madan Unit). Based on these, the nomenclature position of the investigated species has been justified within the recommended by the International Mineralogical Association (IMA) nomenclature of epidote-group minerals (Armbuster *et al.*, 2006, Mills *et al.*, 2009). In the second part, comparisons of certain geometrical and crystallographic parameters derived from the crystal structures of several selected epidotes from the available world literature are made with respect to the content of the transition element in the M3 site. The results obtained for the Bulgarian specimens in the first part of this study are also included in this selection. The objectives of this comparative study are: (i) to indicate the place of the Bulgarian specimens in the nomenclature; (ii) to derive trends and regularities arising from the transition metal content in the M3 position on the selected geometrical and crystallographic parameters of the structure (mainly  $Fe^{3+}$  and hence the dependence on the size of the M3 cation); (iii) to shed light on the effect of Mn content and Mn/Fe ratio on the structural peculiarities of the specimens containing this element.

## GEOLOGICAL SETTINGS AND PREVIOUS MINERALOGICAL STUDIES ON THE TWO BULGARIAN LOCALITIES

### Samurski Dol, Chepelare region, Central Rhodopes

The metamorphic sequence of the Rhodope metamorphic complex in the Chepelare region is characterized by a variegated succession of ortho- and parametamorphic rocks (various gneisses including garnet-kyanite, amphibole-biotite and two-mica; marbles, amphibolites and serpentized ultramafic rocks), part of the Arda lithotectonic unit known as Chepelare mélange (Georgieva *et al.*, 2009, and references therein; Sarov *et al.*, 2006a). Pegmatite dykes with variable width intrude and crosscut the metamorphic rocks (Arnaudov and Petrusenko, 1967). The epidote samples originate from a marble quarry (described by Stavrakieva and Petrusenko, 2005) situated in the SE part of the region, about 1 km east of the town of Chepelare. The metacarbonate rocks are characterized by a large variety of minerals formed by fluid-driven metamorphic reactions and related mass transfer. Calcite marbles generally contain minor micas, quartz, feldspars, diopside, tremolite, titanite, apatite, zircon and graphite, while impure marbles have variable content of silicates (15–45 vol.%, Georgieva *et al.*, 2009). The following minerals have been described from the Samurski Dol area: kyanite (Kostov *et al.*, 1962), sillimanite (Petrusenko, 1968), pink clinozoisite (Petrusenko and Padera, 1970); forsterite, diopside, tremolite, titanite, scapolite (mariallite), anorthite, phlogopite, orthoclase (Stavrakieva and Petrusenko, 2005; Georgieva *et al.*, 2009).

### Altered pegmatite from the area of the Pechinsko Pass, near the Strashimir Pb–Zn vein deposit, Madan ore region, Central Rhodopes

The studied epidote mineralization is a hydrothermal alteration product with a thickness of up to 40 cm, developed in a large (up to 2 m wide) pegmatite dyke and resulted from a late hydrothermal event. The pegmatite body crops out in the area of the Pechinsko Pass, close to the upper part of the Strashimir Pb-Zn vein deposit, Madan district. The pegmatite is emplaced at ~40 Ma (U-Pb titanite age, Georgieva *et al.*, 2021, 2023) along the contact between marbles and gneisses with amphibolite lenses. Together with numerous similar pegmatite bodies, it intrudes the high-grade metamorphic rock succession with Jurassic protolithic age referred

to as the Madan lithotectonic unit (Sarov *et al.*, 2006b, 2010; Raeva and Cherneva, 2008; Raeva *et al.*, 2008; Jahn-Awe *et al.*, 2012) of the Rhodope Metamorphic Complex. The outcrop is situated near the plane of a low-angle subhorizontal fault defined as the Madan detachment (Sarov *et al.*, 2006b), which separates the Madan Unit from the partly migmatized Carboniferous–Permian orthogneisses of the Arda Unit (Cherneva and Georgieva, 2005; Ivanov, 2017). The hydrothermal fluid circulation in the region caused alteration in the aluminosilicate rocks (gneisses, pegmatites) and eventually resulted in ore-precipitation of economic grade base metal mineralization (galena and sphalerite) at ~30 Ma (Ar-Ar on sericite, Kaiser-Rohrmeier *et al.*, 2013) in the Madan district. A distinct geochemical feature of the Central Rhodope Pb-Zn deposits is the increased Mn-content in the components of the hydrothermal system (Vassileva, 2002; Vassileva *et al.*, 2009, Hantsche *et al.*, 2021). The pegmatite host is composed of plagioclase, K-feldspar and minor quantities of quartz. Accessories of Nb-bearing titanite, allanite-(Ce), apatite and zircon are characteristic. In the pegmatite-altering hydrothermal mineralization, epidote associates with chlorite, quartz and minor carbonates. The morphology, mineral association and chemical properties of two well-distinguished epidote generations (pink and green) have been studied in details by Georgieva *et al.* (2021, 2023).

## MATERIALS AND METHODS

The sample from the Samurski Dol locality is currently preserved in the National Museum of Natural History at the Bulgarian Academy of Sciences, Sofia, under the number 8126.

The second locality represents an altered pegmatite outcropping around the Pechinsko Pass near the Strashimir Pb-Zn vein deposit with well-developed late epidote alteration zone. These epidotes, previously classified as members of the clinozoisite–epidote series, are manifested in two well-distinguished texturally, chemically and by color generations (pink and green) in association with chlorite, quartz and carbonates (Georgieva *et al.*, 2023).

### Chemical composition

SEM and EDS analyses of the pink clinozoisite from the Samurski Dol (SD) were carried out, using an X-MaxN 50 mm<sup>2</sup> EDS detector by Oxford Instruments (20 kV accelerating voltage), mounted on

a Tescan Vega 3 XMU electron microscope at the Research and Development Department of Aurubis Bulgaria AD, Pirdop. AZtec Energy software was used for data collection, integration and corrections, using integrated factory standards. The chemical formula (averaged from 20 analyses) of the studied SD sample was calculated based on 12.5 oxygen atoms and 8 cations ( $\Sigma(A+M+Si)$ ) per formula unit.

The epidotes from the altered pegmatite in the area of the Pechinsko Pass (samples PP-1, PP-2 and PP-3 for the pink varieties and PP-4 for the green one) were studied with SEM in BSE-regime by a JEOL JSM-6010PLUS/LA (University of Mining and Geology) and a JEOL JSM-6390 (Institute of Physical Chemistry, BAS) for textural and morphological characteristics, mineral relationships and crystal zoning. The chemical composition of minerals was determined using a Hitachi S-3400N SEM equipped with an Oxford Instruments Energy Dispersive Spectrometer X-Max20 (accelerating voltage 20 kV, beam current 1.7 nA, working distance 10 mm, acquisition time 30 s in spot-mode) at the “Geomodel” Resource Center of St. Petersburg State University. Quantification of elemental compositions was conducted using standard samples of natural and synthetic compounds. The structural formulae of epidote-group minerals were calculated, based on 12.5 oxygen atoms and 8 cations.

### Single-crystal x-ray diffraction analysis (SXDA)

The crystals from the studied samples were mounted on glass capillaries and analyzed by single-crystal diffraction method. Data collections were performed on a Bruker D8 Venture diffractometer. The diffraction patterns observed at SXDA characterize the studied sample as single-phase ones. Determination of unit cell parameters, data integration, scaling and absorption corrections were carried out using an APEX4 program package. The structures were solved by direct methods (SHELXS) and refined by full-matrix least-square procedures on F2 (SHELXL, Sheldrick, 2008). As indicated above, in the crystal structure of the investigated compound, there are three positions of octahedrally coordinated cations (M1, M2, M3), which are occupied predominantly by trivalent metal ions. Chemical analyses of the studied samples suggest that these positions are mainly occupied by Al<sup>3+</sup> and up to 5% Fe<sup>3+</sup> and Mn<sup>3+</sup>. As a first step, a structural model was specified and refined, in which the M1, M2 and M3 positions have been occupied solely by Al<sup>3+</sup>. Next, a refinement of the structural model was done, in which the occupancies of the three octahedral positions

have also been included as non-fixed values. In all investigated samples, M1 and M2 display 100% aluminum occupancy, whereas the M3 position exhibits 110% to 130% occupancy, suggesting that iron and manganese ions may also enter this site together with aluminum. Since the amount of Mn is about twenty times lower than that of Fe and the atoms of both of these elements have very close atomic scattering factors, the occupancy of  $Mn^{3+}$  has been fixed on the basis of the average value of manganese from the chemical analyses. Upon further processing of the structural model, only the occupancies of aluminum and iron have been refined in such a way that the total occupancy of M3 has been assumed to be 100%. A refinement of the isotropic and anisotropic temperature factors follows. Hydrogen atoms have been fixed from the Fourier distribution map of the residual electron density. Additional information about the structural data is available in the Cambridge Structural Database: CSD 2281246, 2281243, 2281245, 2281247, 2281244 for PP-1, PP-2, PP-3, PP-4 and SD, respectively.

### Visualization

The program VESTA ver. 3.3.2 (Momma and Izumi, 2011) was used for graphic presentations, extraction of certain crystallographic and geometric parameters (bond lengths and angles), and calculation of distortion indices (DI), bond angle variances (BAV) and cation polyhedral volumes (PV) for the studied epidotes. In this program, deviations from the perfect values for the measured polyhedra in terms of atomic distances and angles have been defined as follows:

(i) Distortion indices (DI) – a quantitative measure of polyhedral distortion, which is independent of the effective size of the polyhedron:

$$DI = \frac{1}{n} \sum_{i=1}^n \frac{|l_i - l_{av}|}{l_{av}}$$

where  $n$  is the number of faces in the polyhedron;  $l_i$  is the distance from the central atom to the  $i^{\text{th}}$  coordinating atom, and  $l_{av}$  is the average bond length;

(ii) Bond angle variance (BAV):

$$BAV = \sigma^2 = \frac{1}{m-1} \sum_{i=1}^m (\varphi_i - \varphi_0)^2,$$

where  $m$  is (number of faces in the polyhedron)  $\times$  3/2 (*i.e.*, number of bond angles),  $\varphi_i$  is the  $i^{\text{th}}$  bond angle, and  $\varphi_0$  is the ideal bond angle for a regular polyhedron (for example,  $90^\circ$  for an octahedron or  $109^\circ 28'$  for a tetrahedron). The higher the values of these indices, the greater the polyhedral distortions and the greater the degree of structural imperfection.

### Choice of epidotes for the comparative study

In order to fulfil the objectives of this study, a set of criteria for identification of appropriate species have been specified as follows:

- taking into consideration the observed by *Giuli et al.* (1999) linear relation due to  $Al \leftrightarrow Fe^{3+}$  substitution attention has been paid only to representatives of the clinozoisite-epidote series as defined by Mindat.org, *i.e.*, all M sites are occupied by only Al and/or  $Fe^{2+}$  and both A1 and A2 sites are occupied entirely by Ca;

- Crystallographic Information Files (CIF) providing information on the population of only the M3 site with transition metal(s) (predominantly iron) were used in the study, *i.e.*, both M1 and M2 sites are occupied entirely by Al;

- only crystal structural data obtained by X-ray diffraction (both single crystal – SCXRD, and powder – PXRD) have been processed;

- an attempt was made to cover the whole possible compositional range for the M3 site, *i.e.*,  $Al_{1-x}Fe_x$ , ( $0 \leq x \leq 1$ );

- the Bulgarian species were included in this selection because of the very low manganese content in them. In the Pechinsko Pass altered pegmatite samples, Mn does not exceed 0.007 apfu (0.004 on average), and the average value for the Samurski Dol clinozoisite is 0.014 apfu.

Among the CIFs found, there is one containing structural data for a medium-iron epidote with composition  $Ca_2Al_{2.40}Fe_{0.60}Si_3O_{13}H$  from Paranesti, northern Greece, reported by Stergiou *et al.* (1987). This sample CIF meets the above-listed criteria. However, according to the processed structural data this compound behaves like an epidote of higher ferrian content, *e.g.*,  $\approx 0.8Fe$  apfu. Although this fact does not significantly disturb the observed linear trends, this sample has been excluded from the subsequent research.

After the data, collected according to the above criteria, were properly processed in MS Excel, the results were presented in graphs, together with the extracted linear trendlines and  $R^2$  values. Subsequently, data for the  $Mn^{3+}$ -rich epidote group representatives were plotted on them, too. Their selection was made, using criteria as close as possible to those described above. Unlike the predominantly  $Fe^{3+}$ -bearing epidotes,  $Mn^{3+}$ -rich ones contain in their structure larger cations than the titular ones in the corresponding positions, *e.g.*, in A (predominantly in A2) and in M1 and sometimes in M2 (see Mindat.org general formula in the introduction herein, Nagashima and Akasaka, 2004). This fact

further affects the studied trends and makes their unambiguous assessment difficult. Four compounds were selected in this group – one natural and three synthetic phases with minimal contents of cations other than Ca and Al in the above-mentioned sites. The crystal chemical data for the synthetic phases were obtained by Rietveld refinement.

Table 1 provides data for the final selection of epidotes used for this comparative study.

## RESULTS AND DISCUSSION

The clinozoisite from the Samurski Dol locality was observed as deep pink anhedral grains up to 2–3 mm in a matrix of scapolite and oligoclase, as well as muscovite (sericite) as alteration product (Fig. 2). The early generation of the Pechinsko Pass epidotes occurs as sub- to euhedral, short prismatic (up to 5 mm), deep pink to red single crystals or clusters in veins and

Table 1

Provenance of epidote-group representatives, whose crystal structural data have been processed in this work

Sample code	Locality	Reference	Database code
<i>Fe<sup>3+</sup>-containing, Fe<sup>3+</sup>-rich clinozoisites, epidotes</i>			
WNY	Willsboro, New York, USA	Dollase (1968)	ICSD* #9246
SD	Samurski Dol, Bulgaria	This work	
PP-1	Pegmatite, Pechinsko Pass, Bulgaria	This work	
PP-2	Pegmatite, Pechinsko Pass, Bulgaria	This work	
LEP	Tyrol 1, Austria	Gabe <i>et al.</i> (1973)	amcsd* 0000309
PP-3	Pegmatite, Pechinsko Pass, Bulgaria	This work	
PP-4	Pegmatite, Pechinsko Pass, Bulgaria	This work	
VSI-1	Val Sissone, Rhetic Alps, Italy	Gatta <i>et al.</i> (2010)	ICSD #168464
VSI-2	Val Sissone, Rhetic Alps, Italy	Gatta <i>et al.</i> (2012)	ICSD #183753
HEP	Tyrol 2, Austria	Gabe <i>et al.</i> (1973)	amcsd 0000308
UNC**	Unknown locality	Nozik <i>et al.</i> (1978)	ICSD #34209
<i>Mn<sup>3+</sup>-containing, Mn<sup>3+</sup>-rich clinozoisite, epidote, piemontites</i>			
NA-45	synthetic	Nagashima and Akasaka (2004)	ICSD #55238
NA-65	synthetic	Nagashima and Akasaka (2004)	ICSD #55239
NA-69	synthetic	Nagashima and Akasaka (2010)	ICSD #168339
STM	St. Marcel, Italy	Dollase (1969)	ICSD #26354

\* See <https://doi.org/10.18434/M32147> and Downs and Hall-Wallace (2003).

\*\* unknown locality.

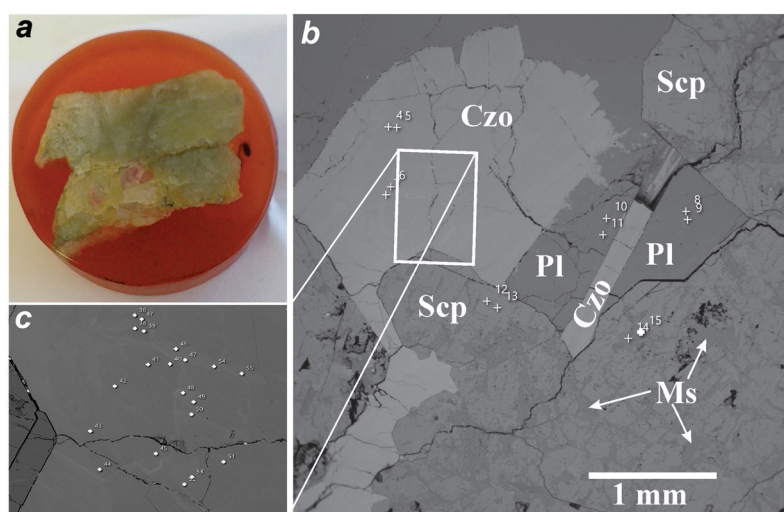


**Fig. 2.** a) Photograph of a polished section with grains of pink clinozoisite from the Samurski Dol locality; b) SEM image of a mineral association of scapolite (Scp) with clinozoisite (Czo) and oligoclase (Pl), and muscovite (Ms) as alteration product; c) sites of the EDS analyses.

nests. The late generation occurs as green, sub- to euhedral, elongated prismatic crystals (up to 5 cm) and radiating aggregates overgrowing or crosscutting the first epidote generation (Fig. 3).

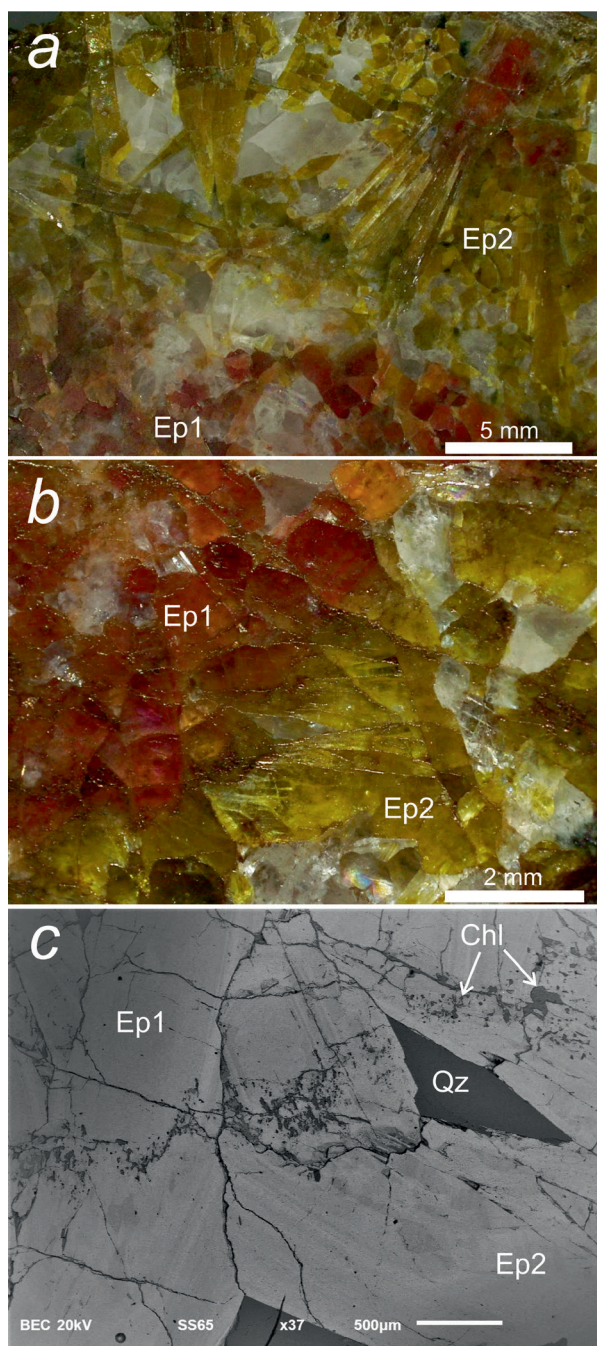


**Fig. 3.** Occurrence of the hydrothermal epidotes in the altered pegmatite from the area of the Pechinsko Pass: *a, b*) stereomicroscopic images of both epidote generations – early pink (Ep1) and late green (Ep2); *c*) BSE image close to the area shown in *b* with a distinct boundary between the two generations, marked by chlorite mineralization. Abbreviations: Qz – quartz; Ep – epidote; Chl – chlorite.

Table 2 presents certain important data collection and refinement parameters for the studied compounds. Table 3 contains selected bond lengths for the studied compounds.

The chemical composition of the SD sample as determined by EDS and its crystal chemical formula is  $\text{Ca}_{2.02-2.09}(\text{Al}_{2.64-2.89}\text{Fe}_{0.13-0.38}\text{Mn}_{0.007-0.03})_{3.02-3.06}[\text{Si}_2\text{O}_7][\text{SiO}_4]\text{O}(\text{OH})$  ( $\text{Si}_{2.99-3.01}$  apfu). Regardless of the slightly increased calcium content and sum of the octahedral cations, calculations applied to the averaged structural formula  $\text{Ca}_{2.06}(\text{Al}_{2.80}\text{Fe}_{0.22}\text{Mn}_{0.01})_{3.03}[\text{Si}_2\text{O}_7][\text{SiO}_4]\text{O}(\text{OH})$  demonstrate a charge balance deviation below 1%, which indicates the reliability of the obtained results. The wide range in which iron and manganese contents vary is most likely due to an uneven supply of these elements during crystal growth, which is also evidenced by the observed sectorial structure of this mineral. Based on these data, supported also by the results from the single-crystal investigations, the SD mineral sample can be defined as  $\text{Mn}^{3+}$ -containing clinzoisite and, taking into consideration its deep pink color, as its mineral variety *clinothulite* (<https://www.mindat.org/min-27132.html>).

According to a previous study (Georgieva *et al.*, 2023), the major element chemical composition of the Pechinsko Pass epidotes reveals members of the clinzoisite-epidote solid solution (Armbruster *et al.*, 2006), predominantly Fe-rich clinzoisite towards epidote in the second generation. Despite the chemical inhomogeneity, the crystal chemical formula of the pink generation, as determined by representative EDS data, ranges as follows:

$\text{Ca}_{1.97-2.01}\text{Mn}_{0.0-0.003}(\text{Al}_{2.47-2.60}\text{Fe}_{0.35-0.48}\text{Mn}_{0.01-0.03})_{2.97-3.00}[\text{Si}_2\text{O}_7][\text{SiO}_4]\text{O}(\text{OH})$  ( $\text{Si}_{3.02-3.03}$  apfu);

whereas, for the green generation, it is

$\text{Ca}_{1.98-2.04}\text{Mn}_{0.005-0.01}(\text{Al}_{2.01-2.50}\text{Fe}_{0.48-0.91}\text{Mn}_{0.0-0.02})_{2.96-3.00}[\text{Si}_2\text{O}_7][\text{SiO}_4]\text{O}(\text{OH})$  ( $\text{Si}_{2.98-3.04}$  apfu).

Based on the crystal chemical data obtained in this study, they can be defined as follows: PP-1 and PP-2 are  $\text{Mn}^{3+}$ -containing clinzoisites (*clinothulites*) and PP-3 and PP-4 can be called  $\text{Mn}^{3+}$ -containing epidotes due to the predominance of  $\text{Fe}^{3+}$  content in one of the octahedral sites (M3) in their structures (Table 2).

Table 4 contains data for the comparative study concerning the  $\text{Fe}^{3+}$ -containing clinzoisite-epidote series members. Column 1 shows the occupation percentages of the three possible cations in the M3 site. The formulation and meaning of the DI and BAV values (columns 2 and 3, respectively) were explained in the previous section. M3 PV (column 9) is the polyhedral (octahedral) volume of the M3 site. The equatorial/apical (eq/ap) parameter

Table 2  
Most important data collection and refinement parameters for the studied compounds

Compound	PP-1	PP-2	PP-3	PP-4	SD
Chemical formula	$\text{Al}_{2.09}\text{Ca}_2\text{Fe}_{0.31}\text{HMn}_{0.002}\text{O}_{13}\text{Si}_3$	$\text{Al}_{2.61}\text{Ca}_2\text{Fe}_{0.39}\text{HMn}_{0.002}\text{O}_{13}\text{Si}_3$	$\text{Al}_{2.48}\text{Ca}_2\text{Fe}_{0.52}\text{HMn}_{0.002}\text{O}_{13}\text{Si}_3$	$\text{Al}_{2.41}\text{Ca}_2\text{Fe}_{0.59}\text{HMn}_{0.002}\text{O}_{13}\text{Si}_3$	$\text{Al}_{2.50}\text{Ca}_2\text{Fe}_{0.09}\text{HMn}_{0.01}\text{O}_{13}\text{Si}_3$
Formula weight	463.18	465.49	469.39	471.13	290(2)
Temperature (K)	290(2)	290(2)	290(2)	290(2)	Monoclinic
Crystal system	Monoclinic	Monoclinic	Monoclinic	Monoclinic	$P2_1/m$
Space group	$P2_1/m$	$P2_1/m$	$P2_1/m$	$P2_1/m$	$P2_1/m$
a (Å)	8.8664(2)	8.8698(4)	8.8808(2)	8.8758(3)	8.8621(3)
b (Å)	5.59440(10)	5.6004(2)	5.61190(10)	5.6126(2)	5.5851(2)
c (Å)	10.1404(3)	10.1404(3)	10.1468(2)	10.1441(4)	10.1328(3)
$\alpha$ (°)	90	90	90	90	90
$\beta$ (°)	115.4670(10)	115.4320(10)	115.4340(10)	115.4140(10)	115.4610(10)
$\gamma$ (°)	90	90	90	90	90
Volume (Å <sup>3</sup> )	454.112(19)	454.91(3)	456.686(16)	456.44(3)	452.82(3)
Z	2	2	2	2	2
$\rho_{\text{calc}}$ (g/cm <sup>3</sup> )	3.387	3.398	3.413	3.428	3.355
$\mu$ (mm <sup>-1</sup> )	2.473	2.583	2.766	2.860	2.188
F(000)	460	462.0	466.0	467.0	455.0
Crystal size (mm <sup>3</sup> )	$0.03 \times 0.02 \times 0.02$	$0.03 \times 0.03 \times 0.02$	$0.03 \times 0.02 \times 0.02$	$0.02 \times 0.02 \times 0.015$	$0.03 \times 0.03 \times 0.02$
Radiation, $\lambda$ (Å)	MoK $\alpha$ $\lambda = 0.71073$	MoK $\alpha$ $\lambda = 0.71073$	MoK $\alpha$ $\lambda = 0.71073$	MoK $\alpha$ $\lambda = 0.71073$	MoK $\alpha$ $\lambda = 0.71073$
$\Theta$ range for data collection (°)	3.992 to 50.696	4.448 to 56.676	4.446 to 56.536	4.446 to 56.636	4.452 to 52.736
Limiting indices	$-11 \leq h \leq 11, -7 \leq k \leq 7, -13 \leq l \leq 13$	$-11 \leq h \leq 11, -7 \leq k \leq 7, -13 \leq l \leq 13$	$-11 \leq h \leq 11, -7 \leq k \leq 7, -13 \leq l \leq 13$	$-11 \leq h \leq 11, -7 \leq k \leq 7, -13 \leq l \leq 12$	$-11 \leq h \leq 10, -6 \leq k \leq 6, -12 \leq l \leq 12$
Reflections collected /unique	11958/1238 [Rint = 0.0331]	10742/1244 [Rint = 0.0362]	10103/1238 [Rint = 0.0307]	9402/1244 [Rint = 0.0255]	7609/1007 [Rint = 0.0292]
Refinement method	Full-matrix least-squares on F <sup>2</sup>	Full-matrix least-squares on F <sup>2</sup>	Full-matrix least-squares on F <sup>2</sup>	Full-matrix least-squares on F <sup>2</sup>	Full-matrix least-squares on F <sup>2</sup>
Data/restraints/parameters	1238/0/120	1244/0/120	1238/0/120	1244/0/120	1007/0/119
Goodness-of-fit on F <sup>2</sup>	1.163	1.087	1.262	1.156	1.229
Final R indexes [I > = 2 $\sigma$ (I)]	R1 = 0.0173, wR2 = 0.0424	R1 = 0.0193, wR2 = 0.0434	R1 = 0.0219, wR2 = 0.0580	R1 = 0.0173, wR2 = 0.0408	R <sub>1</sub> = 0.0183 wR <sub>2</sub> = 0.0465
Final R indexes [all data]	R1 = 0.0194, wR2 = 0.0433	R1 = 0.0224, wR2 = 0.0448	R1 = 0.0237, wR2 = 0.0587	R1 = 0.0180, wR2 = 0.0412	R <sub>1</sub> = 0.0190 wR <sub>2</sub> = 0.0467
Largest diff. peak/hole (e Å <sup>-3</sup> )	0.33/(-0.34)	0.36/(-0.35)	0.48/(-0.43)	0.37/(-0.28)	0.33/(-0.36)

Table 3  
Selected bond lengths (Å) for the studied compounds

Bond*	Bond lengths (Å)				
	PP-1	PP-2	PP-3	PP-4	SD
M1 – O1	2×1.9295(10)	2×1.9312(11)	2×1.9332(15)	2×1.9322(10)	2×1.9269(12)
M1 – O4	2×1.8452(10)	2×1.8432(11)	2×1.8456(14)	2×1.8427(10)	2×1.8470(12)
M1 – O5	2×1.9405(11)	2×1.9435(12)	2×1.9493(15)	2×1.9507(10)	2×1.9354(12)
M2 – O3	2×1.8534(11)	2×1.8523(12)	2×1.8521(15)	2×1.8523(10)	2×1.8543(13)
M2 – O6	2×1.9248(11)	2×1.9231(11)	2×1.9239(16)	2×1.9238(10)	2×1.9243(12)
M2 – O10	2×1.8599(10)	2×1.8585(11)	2×1.8629(15)	2×1.8634(10)	2×1.8546(12)
M3 – O1	2×2.1956(11)	2×2.2028(12)	2×2.2133(17)	2×2.2157(11)	2×2.1879(14)
M3 – O2	2×1.9499(11)	2×1.9566(13)	2×1.9692(17)	2×1.9736(11)	2×1.9363(14)
M3 – O4	1.8896(16)	1.9566(13)	1.9160(20)	1.9191(15)	1.8730(20)
M3 – O8	1.7986(17)	1.8093(19)	1.8240(3)	1.8349(17)	1.7820(20)

\* M1 and M2 – Al<sup>3+</sup>, M3 – Al<sup>3+</sup>, Fe<sup>3+</sup>, Mn<sup>3+</sup>

(column 10) is measured as  $[2(M3 - O1) + 2(M3 - O2)] / (M3 - O4 + M3 - O8)$  (Fig. 1, middle). Si-O-Si (column 11) is the bending angle of the Si<sub>2</sub>O<sub>7</sub>-group (Fig. 1, top). Column 12 contains information about the color of the Bulgarian specimens, supplemented with data on the colors of the other examined specimens, obtained from literature data where available. As can be seen from the data presented in Table 4, the selected samples cover almost evenly the entire possible compositional range for the M3 site, *i.e.*, Al<sub>1-x</sub>Fe<sub>x</sub>, (0 ≤ x ≤ 1). It should also be noted that two of the samples (HEP and UNC) do not fit the observations described by Bonazzi and Menchetti (1995) on the size of the M3 site octahedral volume, respectively its transition element (Fe<sup>3+</sup>) occupancy and the onset of occupancy of the M1 position by this element. In both these samples, iron occupies more than 80% of the M3 sites without detecting its presence in the M1 site and for the UNC specimen the M3 PV exceeds 11 Å<sup>3</sup> (see introduction herein).

Table 5 also contains data for the comparative study concerning Mn<sup>3+</sup>-rich clinozoisite, epidote and piemontites and is organized similarly to Table 4. However, instead of the color column (column 12), two more columns have been inserted, providing information on the, albeit low, values of occupancy by alternative cations (Mn and Fe) in the crystallographic positions M1 and M2.

Figure 4 illustrates the relations of some of the selected geometric and crystallographic parameters on the M3 site composition (Table 4). Sample codes are included only in Fig. 4a, b. All Bulgarian (Mn-containing) samples are designated as red stars (this study's results). The Fe<sup>3+</sup>-containing, Fe<sup>3+</sup>-rich clinozoisites and epidotes are shown as blue circles, and

the Mn<sup>3+</sup>-containing, Mn<sup>3+</sup>-rich clinozoisite, epidote, piemontites – as green squares. The displayed trendlines (dashed lines) are derived based on the data from Table 4 and excluding data for the Mn-rich samples (Table 5). The latter, however, have also been included in the graph through their specific markers. The R<sup>2</sup> values are also presented near the trendlines. The positions of the green markers relative to the trendlines indicate the deviations from the established linear relations of the corresponding samples.

All of the relations concerning the Mn-bearing samples from Bulgaria and Fe-bearing clinozoisites and epidotes (red and the blue markers, correspondingly, shown in Fig. 4) are linear. The R<sup>2</sup> values indicate the degree of reliability of the linear regression model and the dataset used. It is very high for most of the presented relations. It is assumed here that the observed considerable deviations of the selected Mn-rich samples values from the main trendlines are due to the stronger manifestation of the Jahn-Teller effect because of the higher manganese content in these specimens as compared to the rest of the samples used in this study.

Figure 4a illustrates the relation of the eq/ap parameter on the composition of M3 site with increasing amount of transition elements. This parameter has been intentionally introduced because its matching the M3 compositions best represents the Jahn-Teller effect on the octahedral environment of this site. This graph presents the strongest observed linear trend in terms of R<sup>2</sup> and the highest deviations of the Mn<sup>3+</sup>-rich samples' values from the trendline as well. The data are almost identical to those presented in Fig. 4b. The differences arise from the way the two parameters are defined and calculated, and the

Table 4  
 Selected geometric, crystallographic and physical parameters of the studied Fe<sup>3+</sup>-containing, Fe<sup>3+</sup>-rich clinzoisites, epidotes

Sample code	M(3)O6 occupancy, %			BAV, (°) <sup>2</sup>	a, (Å)	b, (Å)	c, (Å)	β, (°)	V, (Å) <sup>3</sup>	M3 PV, (Å) <sup>3</sup>	eq/ap	Si-O-Si, (°)	Color
	Fe	Mn	Al										
	1												
WNY	2.0	–	98	58.06	8.879	5.583	10.155	115.50	454.360	10.009	1.1285	164.30	n.d.
SD	2.0	8.5	89.5	60.62	8.862	5.585	10.131	115.46	452.82	10.097	1.1286	162.44	baker-miller pink
PP-1	30.5	0.2	69.3	64.15	8.866	5.594	10.140	115.47	454.112	10.282	1.1241	160.47	apricot
PP-2	38.5	0.2	61.3	66.46	8.870	5.600	10.140	115.43	454.910	10.405	1.1209	159.19	red-orange coral
LEP	40.0	–	60.0	66.37	8.880	5.604	10.151	115.46	456.150	10.396	1.1195	159.87	pinkish
PP-3	51.8	0.2	48.0	69.55	8.881	5.612	10.147	115.43	456.686	10.590	1.1179	157.52	telemagenta
PP-4	58.6	0.2	41.2	71.61	8.876	5.613	10.144	115.41	456.440	10.656	1.1161	156.73	apple green
VSI-1	71.0	–	29.0	76.05	8.893	5.640	10.185	115.40	458.560	10.848	1.1128	155.45	dark green
VSI-2*	73.0	–	27.0	75.31	8.892	5.621	10.155	115.36	459.060	10.862	1.1109	154.59	dark green
HEP	84.0	–	16.0	74.73	8.890	5.630	10.150	115.38	458.726	10.863	1.1092	154.57	pale green
UNC	100.0	–	–	79.21	8.913	5.643	10.179	115.12	463.540	11.075	1.1055	153.80	n.d.

\* VSI-1 sample was found to contain a negligible amount of 0.001 apfu Fe<sup>3+</sup> in its M1 position.

 Table 5  
 Selected geometric, crystallographic and physical parameters of the studied Mn<sup>3+</sup>-containing, Mn<sup>3+</sup>-rich clinzoisite, epidote and piemontites

Sample code	Mineral type	M(1)O6 occupancy, %			M(2)O6 occupancy, %			M(3)O6 occupancy, %			BAV, (°) <sup>2</sup>	a, (Å)	b, (Å)	c, (Å)	β, (°)	V, (Å) <sup>3</sup>	M3 PV, (Å) <sup>3</sup>	eq/ap	Si-O-Si, (°)
		Fe	Mn	Al	Fe	Mn	Al	Fe	Mn	Al									
		2			3			4											
1		–	–	–	–	–	–	–	–	–	–	–	–	–	–	–	–	–	–
NA-45	Czo	–	1	99	–	4	96	–	45	55	72.92	8.856	5.629	10.148	115.52	456.55	10.764	1.1727	155.90
NA-65	Pmt	–	8	92	–	2	98	–	65	35	77.39	8.853	5.660	10.151	115.51	459.02	10.938	1.1760	151.3
NA-69	Ep	8	2	90	–	–	100	50	19	31	70.54	8.898	5.655	10.175	115.43	462.39	11.279	1.1472	152.28
STM*	Pmt	6	14	80	–	–	100	25	58	17	85.41	8.878	5.692	10.201	115.40	465.66	11.212	1.1449	151.0

\* STM sample was found to contain 0.13 apfu Si<sup>2+</sup> in its A2 position.

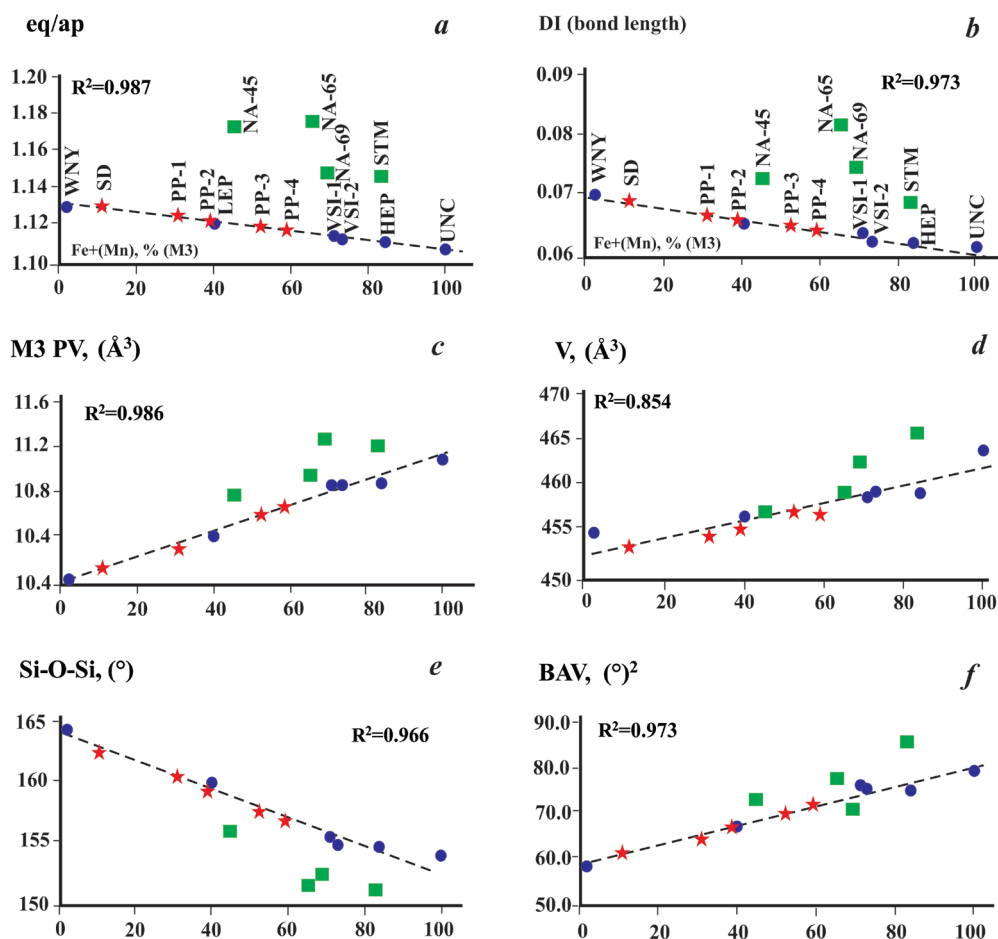


Fig. 4. Relations between selected geometric and crystallographic parameters on the composition of the M3 site.

result is evident in the slightly lowered  $R^2$  value for the DI-relation as calculated by the program VESTA ver. 3.3.2 (Momma and Izumi, 2011). The general trend in both Fig. 4a and Fig. 4b is decreasing. That is, as the ionic radius of the cation increases, the M3 polyhedron increasingly approaches the ideal octahedron in terms of the lengths of the central atom-ligand bonds, *i.e.*, the individual bond length values differ less and less from their average one for this polyhedron. As expected, the values for the  $Mn^{3+}$ -rich samples are higher than the trend, which is related to the increased manganese content and, consequently, the more strongly manifested Jahn-Teller effect and the associated with it axial (apical) compression of the M3 octahedron. The magnitude of the observed deviations depends more or less on the cation fraction of  $Mn^{3+}$  in M3 as well as on the Mn/Fe ratio in this position.

Similar considerations can be made on the relation “volume of the M3 polyhedron – composition of the M3 site” (Fig. 4c). The large difference be-

tween the highest and lowest values for this polyhedron (over 11%), as well as the high  $R^2$  value, indicates that this is the most flexible part in the epidote crystal structure in terms of size of the cations that populate it. Figure 4d illustrates the expected upward trend in the relation “volume of the unit cell – composition of the M3 site”. The data are very similar to those presented in Fig. 4c; however, the  $R^2$  value for them is significantly lower. This fact is interpreted as a manifestation of adaptation of the structure, which responds to the chemical variations in the M3 site by adjusting polyhedral geometry (volume, distortion) and by twisting the linkage between polyhedra – a fact also noted in earlier studies (Giuli *et al.*, 1999, and references therein). Because of the activation of this compensatory mechanism, there are fluctuations in the values of the lattice parameters (Tables 4, 5) and a relatively small increase in the unit cell volume as evidenced by the difference between the highest and lowest values for this parameter (less than 3%). It is note-

worthy that the values of all Bulgarian manganese-containing samples fall below the general trendline, whereas those for the Mn<sup>3+</sup>-rich samples are located above it. This means that, despite the same sizes of their ionic radii, Fe<sup>3+</sup> and Mn<sup>3+</sup> act in a different way on their surroundings, as the Jahn-Teller effect possibly leads to a “shrinkage” of the structure in the region where the (Mn<sup>3+</sup> + Fe<sup>3+</sup>) cation fraction falls below 50% in the M3 position and “extension” is observed where it exceeds this value.

The trend line presented in Fig. 4e illustrates the decrease in the Si-O-Si angle with the increase in the transition element content in the M3 position. This trend is more pronounced for the Mn<sup>3+</sup>-rich samples as evidenced by the deviation of the green markers on the graph and is possibly due to the Jahn-Teller effect. This is a clear manifestation of the response of the structure (the degree of the Si<sub>2</sub>O<sub>7</sub> group bending) to the chemical variations in the M3 site in the structure.

The trendline presented in Fig. 4f is rising. A possible reason for this is the manifestation of an increasingly strong repulsion between the cations in positions M1 (occupied solely by aluminum) and those in M3 with increasing content of transition element(s) in the latter. To test the plausibility of this assumption, measurements of the M1-M1 and M1-M3 lengths (Fig. 1, bottom) of the two end-members of the studied selection presented in Table 4 (the WNY sample with minimum iron content, and the UNC one with maximum content of this element) were made and compared. For the WNY sample, M1-M1 = 2.792 Å and M1-M3 = 2.937 Å. For the UNC specimen, M1-M1 = 2.8215 Å and M1-M3 = 3.003 Å. The differences between the corresponding measured values for the two samples are as follows:  $\Delta(\text{M1-M1})_{(\text{UNC-WNY})} = 0.03 \text{ \AA}$  and  $\Delta(\text{M1-M3})_{(\text{UNC-WNY})} = 0.066 \text{ \AA}$ . The offset between the adjacent purely aluminum M1 positions inferred from the comparison of the two samples is at least half than that occurring between them and the cations populating the M3 site, confirming the assumption made for repulsion due to the increase in ionic radii in M3. An expected consequence of this is the displacement of the central atom of the M3 octahedron from its “ideal” position, and hence the increase in BAV with increasing content of transition elements. The manifestation of the Jahn-Teller effect in this relation is more pronounced for those Mn<sup>3+</sup>-rich samples that do not contain Fe<sup>3+</sup> or at least this element is not the dominant one in the M3 position (e.g., sample NA-69, Table 5).

The data presented in column 12 of Table 4 indicate that, even in small amounts, manganese is an extremely strong chromophore (pink, red, violet,

etc.) even in the presence of higher iron contents. Iron becomes dominant (various green colorations) only when the Fe<sup>3+</sup> >> Mn<sup>3+</sup> or when manganese is totally absent in the samples examined, and Fe<sup>3+</sup> is predominantly present in the M3 position.

## CONCLUSIONS

Mn-containing epidote samples from two Central Rhodope localities were studied. The epidote mineralization is formed by fluid-involved processes after the aluminosilicate (gneiss, pegmatite) and carbonate (marble) rocks from the Madan lithotectonic unit (near Pechinsko Pass, Madan district) and the Arda lithotectonic unit (Chepelare district). Both localities are closely situated to major tectonic zones (Madan detachment, Chepelare shear zone), utilizing fluid transport and fluid-rock interaction. Based on the obtained crystal chemical data, a precise nomenclature position of the investigated species has been justified within the IMA-recommended nomenclature of epidote-group minerals.

The conducted comparative study of the dependence of selected geometrical and crystallographic parameters on the composition of the M3 site in the crystal structure of epidote undoubtedly reveals their linear character when it comes to Fe<sup>3+</sup>-containing, Fe<sup>3+</sup>-rich members of the group. The character of the same dependences for the Mn<sup>3+</sup>-rich samples is more difficult to establish, the main reason being due to the difficulties in finding suitable samples. However, some of the investigated relations, e.g., those of eq/ap- and DI-parameters clearly demonstrate the role of the Jahn-Teller effect in the studied structures of manganese epidotes and more specifically its manifestation as an axial compression of the octahedral environment of the M3 position, which is a preferred site for population by the atoms of this element. The Mn content in the Bulgarian samples is too low to account for its influence in their structures. However, its presence as a strong chromophore is evident here.

## Acknowledgements

The authors thank the National Museum of Natural History staff (Chavdar Karov and Iliya Dimitrov) for providing a fragment of a museum specimen for the current study. The study is partly financially supported by the Bulgarian National Science Fund KP-06-N34/4 project and complements the results of the ERA-MIN PEGMAT project KP-06-DO02/2. We wish to thank the reviewers for their insightful comments. These have greatly helped us to improve the quality of our manuscript.

## REFERENCES

- Armbruster, T., Bonazzi, P., Akasaka, M., Bermanec, V., Chopin, C., Gieré, R., Heuss-Assbichler, S., Liebscher, A., Menchetti, S., Pan, Y., Pasero, M. 2006. Recommended nomenclature of epidote-group minerals. *European Journal of Mineralogy* 18 (5), 551–567, <https://doi.org/10.1127/0935-1221/2006/0018-0551>.
- Arnaudov, V., Petrusenko, S. 1967. Pegmatite mit Moissanit im Kreis Čepelare. *Review of the Bulgarian Geological Society* 28 (2), 203–207 (in Bulgarian, with German abstract).
- Belov, N.V., Rumanova, I.M. 1953. The crystal structure of epidote  $\text{Ca}_2\text{Al}_2\text{FeSi}_3\text{O}_{12}(\text{OH})$ . *Doklady Akademii Nauk SSSR* 89, 853–856.
- Bonazzi, P., Menchetti, S. 1995. Monoclinic members of the epidote group: Effects of the  $\text{Al} \leftrightarrow \text{Fe}^{3+} \leftrightarrow \text{Fe}^{2+}$  substitution and the entry of  $\text{REE}^{3+}$ . *Mineralogy and Petrology* 53, 133–153, <https://doi.org/10.1007/BF01171952>.
- Cherneva, Z., Georgieva, M. 2005. Metamorphosed Hercynian granitoids in the Alpine structures of the Central Rhodope, Bulgaria: geotectonic position and geochemistry. *Lithos* 82 (1–2), 149–168, <https://doi.org/10.1016/j.lithos.2004.12.011>.
- Dollase, W.A. 1968. Refinement and comparison of the structures of zoisite and clinozoisite. *American Mineralogist, Journal of Earth and Planetary Materials* 53 (11–12), 1882–1898.
- Dollase, W.A. 1969. Crystal structure and cation ordering of piemontite. *American Mineralogist, Journal of Earth and Planetary Materials* 54 (5–6), 710–717.
- Downs, R.T., Hall-Wallace, M. 2003. The American Mineralogist Crystal Structure Database. *American Mineralogist* 88, 247–250.
- Gabe, E.J., Portheine, J.C., Whitlone, S.H. 1973. A reinvestigation of the epidote structure: confirmation of the iron location. *American Mineralogist, Journal of Earth and Planetary Materials* 58 (3–4), 218–223.
- Gatta, G.D., Meven, M., Bromiley, G. 2010. Effects of temperature on the crystal structure of epidote: a neutron single-crystal diffraction study at 293 and 1,070 K. *Physics and Chemistry of Minerals* 37, 475–485, <https://doi.org/10.1007/s00269-009-0348-5>.
- Gatta, G.D., Alvaro, M., Bromiley, G. 2012. A low temperature X-ray single-crystal diffraction and polarised infra-red study of epidote. *Physics and Chemistry of Minerals* 39, 1–15, <https://doi.org/10.1007/s00269-011-0455-y>.
- Georgieva, M., Cherneva, Z., Hekimova, S., Petrova, A. 2009. Petrology of marbles from the Arda tectonic unit, Central Rhodope, Bulgaria. *Bulgarian Geological Society, National Conference with International Participation “Geosciences 2009”, Abstracts*, 43–44.
- Georgieva, S., Vassileva, R., Milenkov, G., Stefanova, E., Peytcheva, I. 2021. Epidote metasomatic zone in pegmatites from the vicinity of Strashimir Pb-Zn vein deposit, Central Rhodopes: mineralogy, geochemistry and in-situ U/Pb age determination. *Review of the Bulgarian Geological Society* 82 (3), 22–24, <https://doi.org/10.52215/rev.bgs.2021.82.3.22>.
- Georgieva, S., Vassileva, R.D., Plotkina, Y., Milenkov, G., Grozdev, V., Stefanova, E., Peytcheva, I. 2023. Mineral chemistry and in-situ U-Pb geochronology of altered pegmatite from the vicinity of the Strashimir Pb-Zn vein deposit. *Geologica Balcanica* 52 (2), 29–51, <https://doi.org/10.52321/GeolBalc.52.2.29>.
- Giuli, G., Bonazzi, P., Menchetti, S. 1999. Al-Fe disorder in synthetic epidotes: A single-crystal X-ray diffraction study. *American Mineralogist* 84 (5–6), 933–936, <https://doi.org/10.2138/am-1999-5-630>.
- Hantsche, A.L., Kouzmanov, K., Milenkov, G., Vezzoni, S., Vassileva, R., Dini, A., Sheldrake, T., Laurent, O., Guilong, M. 2021. Metasomatism and cyclic skarn growth along lithological contacts: Physical and geochemical evidence from a distal Pb–Zn skarn. *Lithos* 400–401, 106408, <https://doi.org/10.1016/j.lithos.2021.106408>.
- Ito, T. 1950. *X-Ray Studies on Polymorphism. Chapter 5*. Maruzen Company, Tokyo, 231 pp.
- Ito, T., Morimoto, N., Sadanaga, R. 1954. On the structure of epidote. *Acta Crystallographica* 7, 53–59, <https://doi.org/10.1107/S0365110X54000084>.
- Ivanov, Z. 2017. *Tectonics of Bulgaria*. “St. Kliment Ohridski” University Press, Sofia, 332 pp. (in Bulgarian).
- Jahn-Awe, S., Pleuger, J., Frei, D., Georgiev, N., Froitzheim, N., Nagel, T. 2012. Time constraints for low-angle shear zones in the Central Rhodopes (Bulgaria) and their significance for the exhumation of high-pressure rocks. *International Journal of Earth Sciences* 101, 1971–2004, <https://doi.org/10.1007/s00531-012-0764-5>.
- Jahn, H.A., Teller, E. 1937. Stability of polyatomic molecules in degenerate electronic states. I. Orbital degeneracy. *Proceedings of the Royal Society of London A* 161 (905), 220–235, <https://doi.org/10.1098/rspa.1937.0142>.
- Kaiser-Rohrmeier, M., von Quadt, A., Driesner, T., Heinrich, C.A., Handler, R., Ovtcharova, M., Ivanov, Z., Petrov, P., Sarov, S., Peytcheva, I. 2013. Post-orogenic extension and hydrothermal ore formation: High-precision geochronology of the Central Rhodopian metamorphic core complex (Bulgaria–Greece). *Economic Geology* 108 (4), 691–718, <https://doi.org/10.2113/econgeo.108.4.691>.
- Kostov, I., Ivanov, I., Petrusenko, S. 1962. The distene occurrence at the village of Čepelare, Smolyan region. *Bulletin of the Geological Institute, Series Geochemistry, Mineralogy and Petrography* 3, 69–92 (in Bulgarian, with English abstract).
- Langer, K., Tillmanns, E., Kersten, M., Almen, H., Arni, R.K. 2002. The crystal chemistry of  $\text{Mn}^{3+}$  in the clino- and ortho-zoisite structure types,  $\text{Ca}_2\text{M}_2^{3+}[\text{OH}|\text{O}|\text{SiO}_4|\text{Si}_2\text{O}_7]$ : A structural and spectroscopic study of some natural piemontites and “thulites” and their synthetic equivalents. *Zeitschrift für Kristallographie – Crystalline Materials* 217 (11), 563–580, <https://doi.org/10.1524/zkri.217.11.563.20780>.
- Mills, S.J., Hatert, F., Nickel, E.H., Ferraris, G. 2009. The standardisation of mineral group hierarchies: application to recent nomenclature proposals. *European Journal of Mineralogy* 21 (5), 1073–1080, <https://doi.org/10.1127/0935-1221/2009/0021-1994>.
- Momma, K., Izumi, F. 2011. VESTA 3 for three-dimensional visualization of crystal, volumetric and morphology data. *Journal of Applied Crystallography* 44, 1272–1276, <https://doi.org/10.1107/S0021889811038970>.
- Nagashima, M., Akasaka, M. 2004. An X-ray Rietveld study of piemontite on the join  $\text{Ca}_2\text{Al}_3\text{Si}_3\text{O}_{12}(\text{OH})$ – $\text{Ca}_2\text{Mn}_3^{3+}\text{Si}_3\text{O}_{12}(\text{OH})$  formed by hydrothermal synthesis. *American Mineralogist* 89 (7), 1119–1129, <https://doi.org/10.2138/am-2004-0725>.
- Nagashima, M., Akasaka, M. 2010. X-ray Rietveld and  $^{57}\text{Fe}$  Mössbauer studies of epidote and piemontite on the join  $\text{Ca}_2\text{Al}_2\text{Fe}^{3+}\text{Si}_3\text{O}_{12}(\text{OH})$ – $\text{Ca}_2\text{Al}_2\text{Mn}^{3+}\text{Si}_3\text{O}_{12}(\text{OH})$  formed by

- hydrothermal synthesis. *American Mineralogist* 95 (8–9), 1237–1246, <https://doi.org/10.2138/am.2010.3418>.
- Nozik, Y.Z., Kanepit, V.N., Fykin, L.Y., Makarov, Y.S. 1978. A neutron-diffraction study of the structure of epidote. *Geochemistry International* 15, 66–69.
- Petrussenko, S. 1968. Sillimanite veins in garnet-distene schists. *Bulletin of the Geological Institute, Series Geochemistry, Mineralogy and Petrography* 17, 201–208 (in Bulgarian, with English abstract).
- Petrussenko, S., Padera, K. 1970. Pink clinozoisite from the Central Rhodopes. *Bulletin of the Geological Institute, Series Geochemistry, Mineralogy and Petrography* 19, 133–138 (in Bulgarian, with English abstract).
- Raeva, E., Cherneva, Z. 2008. Geochemistry of migmatite–granite connection: a case study from the Central Rhodope, Bulgaria. *Geologica Balcanica* 37 (1–2), 53–59, <https://doi.org/10.52321/GeolBalc.37.1-2.53>.
- Raeva, E., Peytcheva, I., Ovtcharova, M., Cherneva, Z. 2008. U-Pb zircon dating of granites and orthogneisses from the Madan unit in the Arda river valley, Central Rhodopes, Bulgaria. *Bulgarian Geological Society, National Conference with International Participation “Geosciences 2008”*, Abstracts, 37–38.
- Sarov, S., Voynova, E., Moskovski, S., Jelezarski, T., Naydenov, K., Nikolov, D., Georgieva, I., Petrov, N., Markov, N. 2006a. *Geological map of the Republic of Bulgaria in scale 1:50 000, map sheet Chepelare*. Ministry of Environment and Water, Bulgarian National Geological Survey, Sofia.
- Sarov, S., Voynova, E., Moskovski, S., Jelezarski, T., Naydenov, K., Nikolov, D., Georgieva, I., Petrov, N., Markov, N. 2006b. *Geological map of the Republic of Bulgaria in scale 1:50 000, map sheet Madan*. Ministry of Environment and Water, Bulgarian National Geological Survey, Sofia.
- Sarov, S., Voynova, E., Ovtcharova, M., Naydenov, K., Georgiev, N., Dimov, D. 2010. Lithotectonic subdivision of the metamorphic rocks in Rila-Rhodope region. *Bulgarian Geological Society, National Conference with International Participation “Geosciences 2010”*, p. 121 (in Bulgarian).
- Shannon, R.D. 1976. Revised effective ionic radii and systematic studies of interatomic distances in halides and chalcogenides. *Acta Crystallographica* A32, 751–767, <https://doi.org/10.1107/S0567739476001551>.
- Sheldrick, G.M. 2008. A short history of SHELX. *Acta Crystallographica* A64, 112–122, <https://doi.org/10.1107/S0108767307043930>.
- Stavrakeva, D., Petrusenko, S. 2005. Mineral composition of the forsteritic marble from Samurski Dol, Chepelare region, central Rhodopes, Bulgaria. *Proceedings of the Jubilee International Conference “80 Years Bulgarian Geological Society”*, 83–86.
- Stergiou, A.C., Rentzeperis, P.J., Sklavounos, S. 1987. Refinement of the crystal structure of a medium iron epidote. *Zeitschrift für Kristallographie – Crystalline Materials* 178 (1–4), 297–306, <https://doi.org/10.1524/zkri.1987.178.14.297>.
- Vassileva, R.D. 2002. *Manganoan skarns from the Central Rhodope Pb-Zn deposits*. PhD thesis, Geological Institute, Bulgarian Academy of Sciences, Sofia, 202 pp. (in Bulgarian).
- Vassileva, R.D., Atanassova, R., Bonev, I.K. 2009. A review of the morphological varieties of ore bodies in the Madan Pb-Zn deposits, Central Rhodopes, Bulgaria. *Geochemistry, Mineralogy and Petrology* 47, 31–49.